



A CFD study on the performance of a passive ocean plastic collector under rough sea conditions



Heiu-Jou Shaw^a, Wen-Lih Chen^{b,*}, Yueh-Heng Li^b

^a Department of System and Naval Mechatronic Engineering, National Cheng Kung University, Tainan, 701, Taiwan

^b Department of Aeronautics and Astronautics, National Cheng Kung University, Tainan, 701, Taiwan

ARTICLE INFO

Keywords:

Ocean plastic collection
CFD
Turbulence model
Current speed
Wave height

ABSTRACT

In this study, a commercial CFD code, STARCCM+, is used to analyze the performance of a passive ocean plastic collector under rough sea conditions. The CFD code was first validated by comparing with data from a scaled model experiment conducted in the towing water tank in National Cheng Kung University, and it was proven to return accurate catch rate. Then thirty-eight test cases were setup to investigate the effects of four different parameters, namely, ocean current speed, wave height, wave length, and plastic density, on the plastic collector's catch rate, which is the percentage of incoming plastic debris intercepted by the plastic collector. It was found that the parameters of wave length and plastic density posed very little effect on catch rate. In contrast, the effects of the other two parameters were significant. Two important thresholds were found, and they were ocean current speed of 2.5 ms^{-1} and wave height of 0.4 m. The catch rate remained at high level until these thresholds were reached. The information found in this study is invaluable for the design of a practical passive ocean plastic collector.

1. Introduction

After World War II, plastic has become an essential material for modern societies, and our ways of life cannot go on without it. It has been used far and wide in almost every aspect of our activities thanks to its many advantages such as very light and durable, strong, very cheap to make, ...etc. As a result, the production of plastic has been sky rocketing especially during the past few decades. Today, we produce more than 400 million tons of plastic every year, which is about the same weight as the entire human population (Plastic Europe, 2013 and Staedter, 2017). Although plastic waste is recycled, a portion of which has entered and accumulated in our seas and oceans, and ocean plastic junk has increasingly become a very serious problem, especially for the marine ecosystem (Perkin, 2015). Some of these plastic debris are caught by giant ocean currents called "gyres" and have concentrated at some specified regions around the world. One of such regions, the most famous one, is called "Great Pacific Garbage Patch", located between Hawaii and California (Parker, 2014; Lebreton et al., 2018). Every year, millions of sea birds and hundreds of thousands of marine animals die because of the ocean plastic pollution. A good example showing how much plastic debris have poisoned our oceans is Henderson Island,

which is a very remote island located between New Zealand and Chile. The island used to be reputed as the last pristine piece of land on earth. But now its shore has become one of the most plastic-polluted coasts in the world. The plastic density is about 671.6 pieces per square meter, which is much higher than the world average value of 239.4 piece per square meter (Lavers and Bond, 2017).

Ocean plastic debris can also produce hazards to our health through food chain. Small pieces of plastic debris can easily be mistakenly eaten by fish, resulting in harmful chemical being transferred through the food chain, which ends up consumed by human and causes damage to our health (Derraik, 2002). Hence, this problem concerns not just the lives of millions of marine animals but also the welfare of ourselves. In addition, these plastic debris also cause staggering economic losses in fishing industry and damages to ocean vessels. It is estimated that such economic loss is \$1.27 billion in APEC region alone annually.

In many developed countries, after years of industrialization, countless tons of debris, including metal, plastic, glass, clothes, ...etc. have been dump into seas and oceans. Among these different kinds of debris, plastic debris is the majority. Fig. 1 shows tons of plastic junk littered on a stretch of coast of Peng-Hu island, which is located at latitude 22.33 north and longitude 119.35 east. Such huge amount of debris is now suffocating fragile marine ecosystem and poisoning fishing

* Corresponding author.

E-mail address: wlichen@mail.ncku.edu.tw (W.-L. Chen).

<https://doi.org/10.1016/j.oceaneng.2019.106243>

Received 27 March 2019; Received in revised form 14 June 2019; Accepted 30 July 2019

Available online 2 August 2019

0029-8018/© 2019 Elsevier Ltd. All rights reserved.

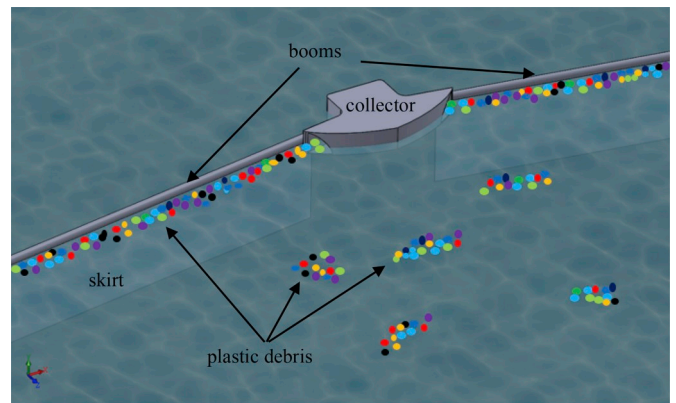
Nomenclature			
A_p	particle projection area (m^2)	V	volume (m^3)
C_d	particle drag coefficient	v_p	particle velocity vector (ms^{-1})
F	force (N)	x_i	Cartesian coordinate in i -direction
f_1	blending factor in k - ω SST model	<i>Greek</i>	
h_0	wave height (m)	α	volume of fluid
I_p	particle inertia momentum ($kgms^{-1}$)	β	coefficient in k and ω equations
k	turbulence kinetic energy (m^2s^{-2})	ρ	density (kgm^{-3})
L_p	particle angular momentum ($kgms^{-1}$)	σ_k, σ_ω	coefficients in k and ω equations
m	mass (kg)	μ	dynamic viscosity (Pas)
P_k	production term in k - ω SST model	μ_t	turbulence viscosity (Pas)
p	pressure (Nm^{-2})	λ	thermal conductivity ($Wm^{-1}K^{-1}$)
t	time (s)	γ	coefficient in ω equation
u_i	velocity components (ms^{-1})	ω	specific energy dissipation rate (s^{-1})
		ω_p	particle angular velocity (s^{-1})



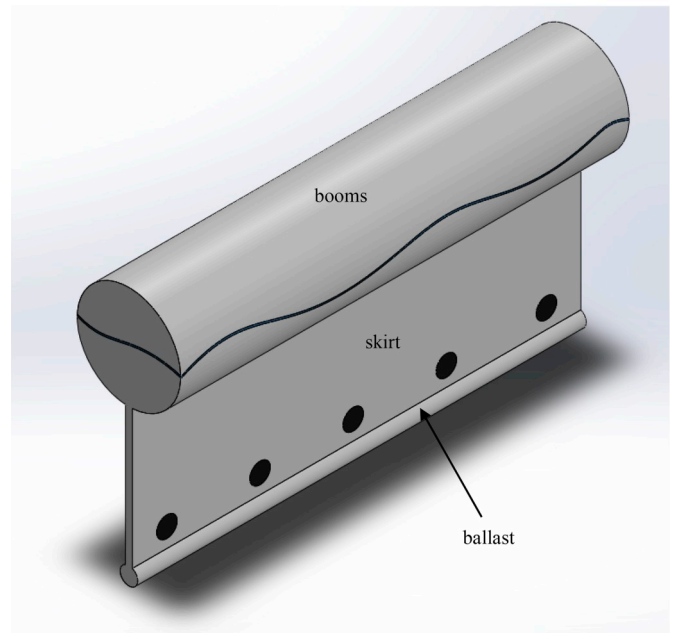
Fig. 1. Ocean plastic debris washed up ashore in Taiwan.

products. As fish is an important part in our diet, everyone’s health is at risk. The ocean plastic problem has become so serious today, we can no longer turn a blind eye on this problem. Some clean-up acts must be planned and executed to significantly reduce the amount of ocean plastic debris.

Conventional ocean plastic debris clean up techniques are based on vessels or divers with nets, which simply “fish” plastic debris out of the ocean. However, in North Pacific Gyre alone, plastic debris spread over an area covering millions of square kilometers. Conventional techniques will take thousands of years and spending billions of dollars to clean up (Moore and Phillips, 2011). Furthermore, conventional techniques also create by-catch and CO₂ emission problems, which can largely offset the benefit of cleaning the ocean. An innovative cleanup concept is “why moves through the oceans if the oceans can move thorough you?“. This concept was first proposed by Boyan Slat, who is the CEO of “The Ocean Cleanup Foundation. Under the framework of this concept, a “passive cleanup” idea has been proposed which features an array of floating barriers anchored on ocean floor to capture plastic debris as it carried by natural ocean currents (Slat, 2014). Fig. 2 illustrates the proposed cleanup system by The Ocean Cleanup Foundation, which consists of several collection stations and some floating barriers stretching over 100 km long. A floating barrier, in this case, is basically a floating boom with a skirt extending some depth under water surface (Fig. 2 (b)). The system will intercept and concentrate floating plastic debris towards the collection stations where plastic debris is extracted out of the ocean and



(a) Overall view



(b) Components of a boom

Fig. 2. Schematic of a passive ocean plastic collector designed by Ocean Cleanup Foundation; (a) overall view, (b) components of a boom.

temporarily stored. A collection vessel will be scheduled to visit these collection stations to collect all the debris and transport it back to land to be further processed. It is estimated that the plastic debris at North Pacific Gyre will be cleaned in a short period of 5 years by this method. A number of small-scale trials have been conducted and gained some success. This method can be deployed in any sea or ocean with strong ocean current. For example, in Taiwan, there is strong Kuroshio Current passing the portion of Pacific Ocean offshore the eastern coast and Southern China Sea Current passing Taiwan Strait, both of which can be explored to clean up ocean plastic debris surrounding Taiwan. The main advantages of passive ocean array collection method are: 1. Operation cost will be drastically reduced compared with conventional vessel and net methods, making the plan more viable. 2. The collected plastic can be converted into energy, oil or new materials to partially offset the operational cost of the ocean array. 3. Since there is no net, there will be no by-catch problem, and no harm will be done to the marine ecosystem.

Computational Fluid Dynamics (CFD) has been widely used to study problems associated with free surface and ocean flows such as marine engineering, wave energy conversion, marine pollution etc. Gaur and Deo (2008) developed a computational tool for forecasting real-time waves in the ocean. Wave information is vital for the operation of any ocean activity; hence, the technology developed by this study is very important. Atan et al. (2019) employed CFD to study the impact on nearshore wave climate imposed by arrays of wave energy converters. It was concluded that arrays of wave energy converters only reduced wave power by less than 1% at a distance between 1 and 3 km from the shore, and the reduction was even much less, at level of 0.1–0.2%, at a distance of 100–300 m from the shore. This study implied using wave energy converters for renewable energy poses little effect of nearshore wave climate. Hamza et al. (2015) used CFD to investigate the dispersion of water pollution by a point source discharged into the coast of Tunisia. They found the damage of such pollution on ecosystems is very serious. The CFD study helped them to plan some measures to limit the degree of degradation of the environment. The above studies demonstrate the usefulness of employing CFD for studying various marine engineering problems.

The Ocean Cleanup Foundation have conducted some CFD studies and performed some experiments to prove the effectiveness of an ocean cleanup array (Slat, 2014). Although many parameters, such as diameter and density of debris, release depth, speed of ocean current, boom angle, tilt angle, have been investigated in these CFD studies, many important factors have not been considered yet. For example, these studies ignore the effects of winds and waves; all plastic particles are assumed to be spherical; only low current speeds, up to 0.15 ms^{-1} , have been examined. That is, only calm sea conditions have been investigated. In some ocean conditions, high waves and winds can drive plastic debris to flow across the floating boom and seriously compromise the catch rate of debris. Furthermore, a plastic debris is rarely spherical in shape, and its geometry is usually irregular. Hence, an ocean cleanup array designed based on the results of these studies could perform not as well as expected. More elaborated CFD modeling is needed to help design a cleanup array that can perform in both calm and rough sea conditions. In this study, we employed a CFD method, which considers wind and wave effects, and simulated the behaviors of irregular plastic debris. Both calm and rough sea conditions were investigated. An ocean plastic collector was designed, and its performance was investigated through the CFD method. The goal is to obtain useful information for designing an ocean cleanup array which can perform well in real sea conditions.

2. Mathematical model

The ocean cleanup collector problem involves multiple mediums, water and air, and multiple phases, gas, liquid, and solid. Some free surface model must be incorporated to simulate waves and their interaction with the collector's solid structure, namely boom, skirt, and ballast. Moreover, the interactions between plastic particles and fluid

medium, plastic particles themselves, and plastic particles and collector structure need be considered to accurately estimate plastic particles' trajectories, and the trajectories of all plastic particles must be traced to calculate how many particles are captured by the array and how many have escaped. Since the scale of an ocean cleanup collector is very large, the fluid flow is turbulent, hence turbulence modeling is required. With so many different mediums and physical mechanisms at play, the physical model is highly complicated. In this study, the fluid flow is governed by Reynolds averaged Navier-Stokes equations, and SST $k-\omega$ model (Menter, 1994), which has been proven to perform well in many industrial flows (Menter et al., 2003), has been adopted for turbulence modeling. The plastic collector is assumed to be rigid and is firmly anchored on the ocean floor so that it cannot move with the waves. Transport equation of Volume of fluid (VOF) is solved to simulate free surface. Hence, the fluid governing equations can be expressed as:

Continuity equation:

$$\frac{\partial \rho}{\partial t} + \frac{\partial}{\partial x_i} (\rho u_i) = 0 \quad (1)$$

Momentum equation:

$$\frac{\partial (\rho u_i)}{\partial t} + \frac{\partial}{\partial x_j} (\rho u_j u_i) = -\frac{\partial p}{\partial x_i} + \frac{\partial}{\partial x_j} \left[(\mu + \mu_t) \frac{\partial u_i}{\partial x_j} \right] \quad (2)$$

VOF equation:

$$\frac{\partial (\rho \alpha)}{\partial t} + \frac{\partial}{\partial x_i} (\rho u_i \alpha) = -\alpha \frac{D\rho}{Dt} \quad (3)$$

where $\alpha = \frac{V_{water}}{V_{total}}$ is volume fraction of water. A cell with $\alpha = 0$ means complete air cell, and a cell with $\alpha = 1$ means complete water cell. Location of free surface is marked by the iso-surface of $\alpha = 0.5$. All fluid properties are calculated using weighting based on α , for example, density is calculated by: $\rho = \rho \alpha_{water} + \rho_{air}(1 - \alpha_{water})$.

The $k-\omega$ SST models incorporates a blending factor, allowing the model to utilize the original $k-\omega$ model of Wilcox (1988) in the inner region of the boundary layer and to switch to the standard $k-\epsilon$ model in the outer region. The k and ω equations are:

Turbulence kinetic energy equation:

$$\frac{\partial \rho k}{\partial t} + \frac{\partial \rho u_j k}{\partial x_j} = P_k - \beta^* \rho k \omega + \frac{\partial}{\partial x_j} \left[(\mu + \sigma_k \mu_t) \frac{\partial k}{\partial x_j} \right] \quad (4)$$

ω equation:

$$\begin{aligned} \frac{\partial \rho \omega}{\partial t} + \frac{\partial \rho u_j \omega}{\partial x_j} &= \gamma P_\omega - \beta \rho \omega^2 + \frac{\partial}{\partial x_j} \left[(\mu + \sigma_\omega \mu_t) \frac{\partial \omega}{\partial x_j} \right] \\ &+ 2\rho(1 - f_1) \sigma_{\omega 2} \frac{1}{\omega} \frac{\partial k}{\partial x_j} \frac{\partial \omega}{\partial x_j}. \end{aligned} \quad (5)$$

In the above equations, coefficients are obtained by the following general formula:

$$\varphi = f_1 \varphi_1 + (1 - f_1) \varphi_2 \quad (6)$$

The above equation shows how the constants (σ_k , σ_ω , γ , β , ...) in the SST $k-\omega$ model are derived. φ_1 stands for the constants in the $k-\omega$ model, φ_2 represents the constants in the $k-\epsilon$ model, and φ represents the corresponding constants of the SST $k-\omega$ model.

Plastic debris are treated as a group of solid particles with different geometries and material properties, and the motion of each particle is calculated by Lagrange based discrete element method (DEM) (Cundall and Strack, 1979). In this method, the interactions among particles themselves and with solid boundaries are considered. Hence, it can simulate the behaviors of plastic particles more accurately. The momentum balance equation of a DEM particle is:

$$m_p \frac{dv_p}{dt} = F_s + F_g + F_c \quad (7)$$

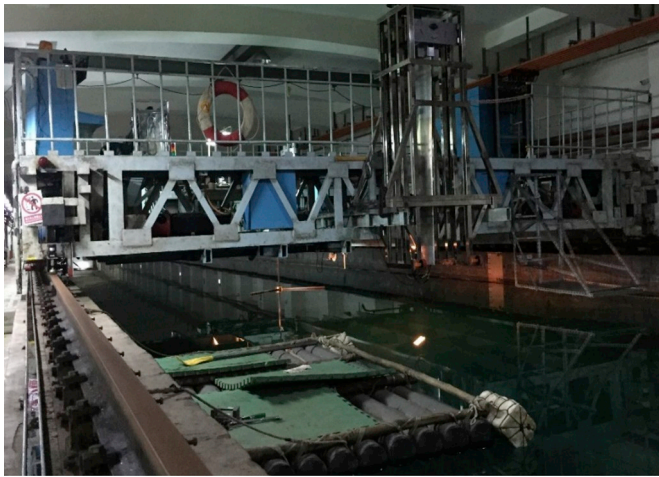


Fig. 3. The towing water tank in NCKU.

where m_p , v_p , F_s , F_g , and F_c are respectively particle's mass, velocity, surface force, gravity force, and contact force. Particle's surface force includes drag force, pressure gradient force, and virtual mass force:

$$F_s = F_d + F_p + F_{vm} \quad (8)$$

These three forces are expressed as:

$$\begin{aligned} F_d &= \frac{1}{2} C_d \rho A_p |v_s| v_s \\ F_p &= -V_p \nabla p_s \\ F_{vm} &= C_{vm} \rho V_p \left(\frac{Dv}{Dt} - \frac{dv_p}{dt} \right) \end{aligned} \quad (9)$$

where C_d , ρ , A_p , v_s , V_p , p_s , C_{vm} are respectively drag coefficient, density of fluid phase, projection area of the particle, slip velocity, particle volume, fluid static pressure, virtual mass coefficient. The contact force is:

$$F_c = \sum_{\text{neighbor particles}} F_{\text{contact}} + \sum_{\text{neighbor boundaries}} F_{\text{contact}} \quad (10)$$

Due to the irregular geometry of a solid particle, rotation can occur while the particle is translating; hence rotation effects need to be considered. The angular momentum equation of a solid particle can be written as:

$$\frac{d}{dt} L_p = \frac{d}{dt} (I_p \omega_p) = \sum_{\text{neighbor particles}} T_{\text{contact}} + \sum_{\text{neighbor boundaries}} T_{\text{contact}} \quad (11)$$

where the contact torque is:

$$T_{\text{contact}} = r_c \times F_{\text{contact}} - \mu r |r_c| |F_{\text{contact}}| \frac{\omega_p}{|\omega_p|} \quad (12)$$

In equation (12), L_p , I_p , r_c , μ_c , and ω_p are respectively particle's angular momentum, inertia momentum, the distance between particle's mass center to contact force, rolling friction coefficient, and angular velocity.

3. Experimental setup

The CFD code used in this study is STARCCM⁺. A scaled-model experiment has been conducted using the towing water tank in National Cheng Kung University to obtain data for validating the CFD code. Fig. 3 shows the towing water tank. This tank is 8 m in width, 4 m in depth, and 176 m in length. A schematic of experimental setup is shown in Fig. 4. The main components of the setup are a scaled collector model, a towing platform, a wave height meter, two cameras, scaled model rigs and elevator, a plastic particle release device, and light bulbs. The scaled model was fixed underneath a towing platform and was towed along the towing water tank to simulate the flow of ocean current, meanwhile, a wave machine produced a series of waves to simulate ocean waves. A schematic of the scaled collector model is illustrated in Fig. 5. The model consists of a main body and two booms on either side of the body. The

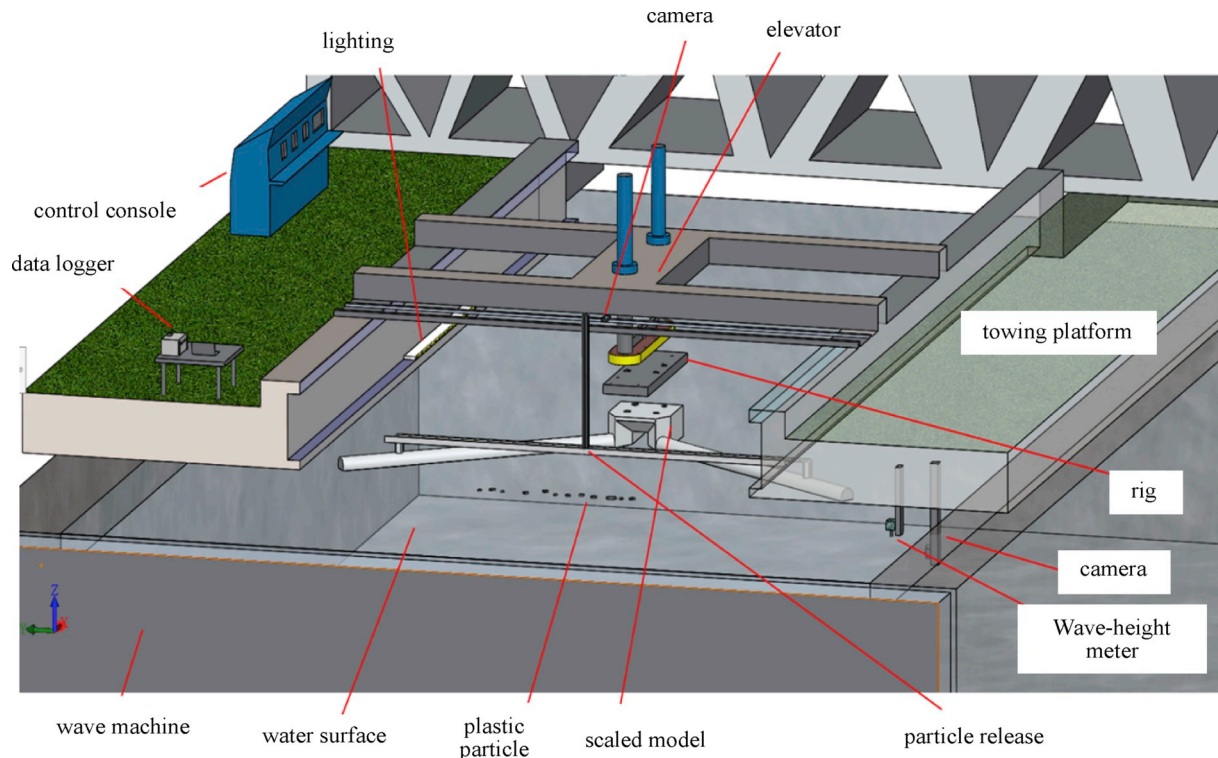


Fig. 4. Schematics of the experimental setup.

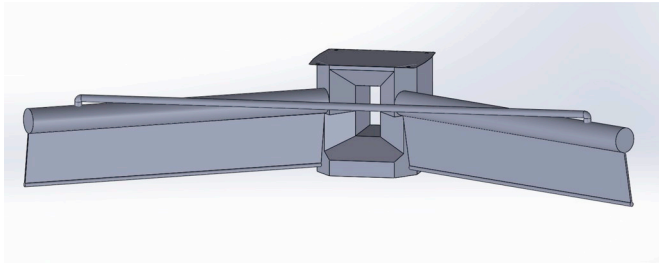


Fig. 5. A schematic of the scaled model of ocean plastic collection array.

main body is a hexagon with width, length, and depth of 0.285 m, 0.285, and 0.315 m, respectively. There is a rectangular hole with 0.07 m in width and 0.14 m in height in the middle of the main body to serve as the collection hole for plastic particles. Once a plastic particle has passed this hole, the particle is regarded as been successfully collected. Each of the two booms is a cylinder with a metal sheet, which is to simulate collection skirt, attached underneath, and the boom angle is 35°. The diameter and the length of the cylinder are 0.072 m and 0.9 m, respectively; and the length and width of the metal sheet are 0.9 m and 0.12 m, respectively. The metal sheet is tilted 10° backwards to simulate the effect of water pressure on collection skirt. There is a support bar connecting the two booms to maintain their relative positions under the force of water current and waves during the experiment.

During an experiment, the towing platform towed the scaled model until a constant speed is reached, then plastic particles were released, and their tracks were recorded until they either passed the scaled model's collection hole or escaped under the scaled model. Between two experiments, there was a 30-min calming period allowing water waves to die down.

The experimental conditions are as follows: towing platform speed was 0.4 ms⁻¹, wave height was 0.05 m, wave period was 1.6 s, and the draft on the boom cylinder was 0.036 m. Under these conditions, some waves can flow over the collector's arms to simulate the effects of rough sea conditions encountered by a real ocean collector. Consistent wave height is very important for this experiment; hence a wave height meter was installed to monitor the variation of wave height. A fragment of wave height reading is given in Fig. 6. The averaged heights of hill and valley are 0.0270 m and 0.0266 m, respectively; and the mean derivations of these two quantities are 8.13% and 6.60%, respectively. As the derivations are less than 10%, the wave height can be considered as reasonably consistent.

The plastic particles in this experiment are spheres with a diameter of

0.03 m and density of 900 kgm⁻³. There were 4 release positions termed position 1, 2, 3, and 4; and they are located at the centerline of the model, 0.2 m, 0.4 m, and 0.65 m deviations from the centerline, respectively.

4. Results and discussion

4.1. CFD code validation

Fig. 7 shows the computation domain of the scaled model. The front surface is the inlet, the rear surface is the outlet, the bottom and lateral surfaces are walls. The water depth is 3.5 m which is the same as the

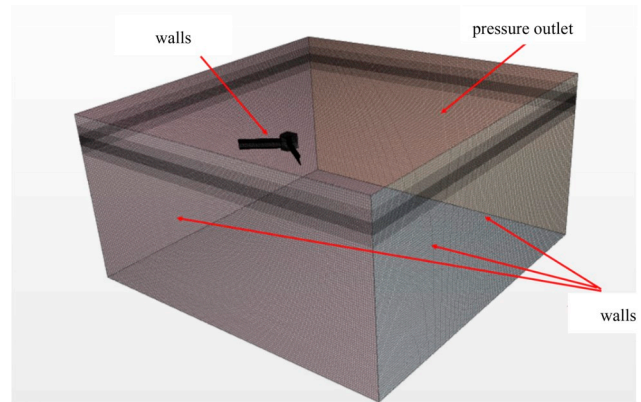


Fig. 7. Computation domain of the scaled model.

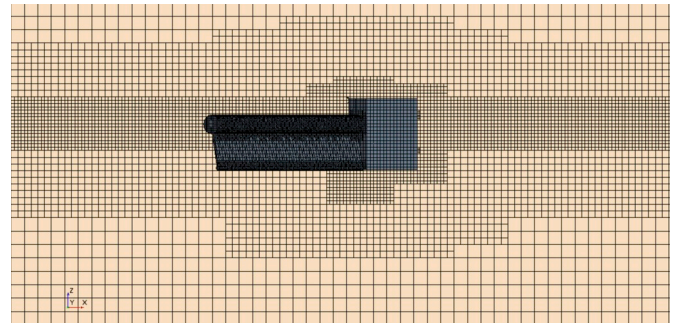


Fig. 8. A cross section of the scaled model's mesh.

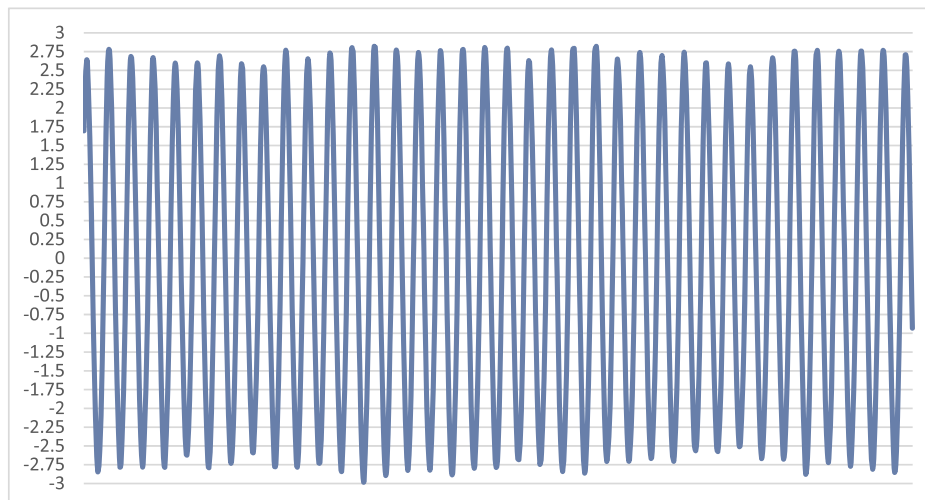
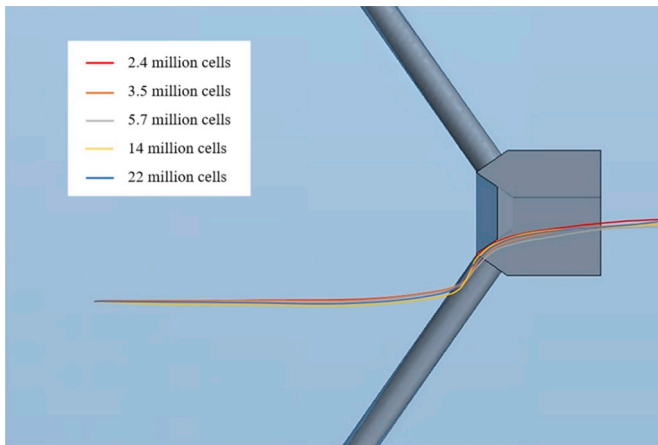
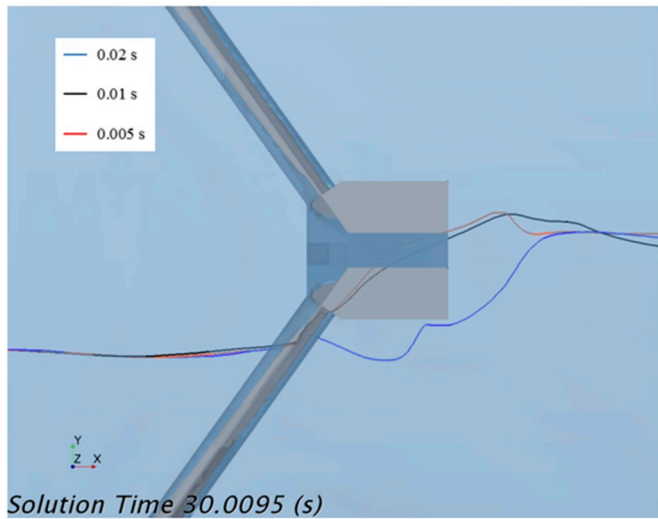


Fig. 6. A fragment of wave height reading.



(a) Using different meshes



(b) Using different time-step intervals

Fig. 9. Comparison of particle tracks by different meshes and time-step intervals; (a) using different meshes, and (b) using different time-step intervals.

experiment. A cross section of the computational mesh is given in Fig. 8. Finer mesh density is concentrated towards the free surface and the plastic collector.

Before the numerical results can be compared with experimental data, grid and time-step-interval independence tests were conducted to find a proper mesh and time-step interval for the CFD simulation on this problem. Five different meshes with time-step interval fixed at 0.01 s and cell numbers of 2,400,000, 3,500,000, 5,700,000, 14,000,000, and 22,000,000, respectively have been tested. Fig. 9 (a) illustrates the tracks of a plastic particle released at the same position by these meshes. Three It can be noted that all tracks are very close, especially the tracks by 5,700,000, 14,000,000, and 22,000,000 cells. This indicates that particle track is not very sensitive to mesh density, and the mesh of 5,700,000 cells is fine enough to return grid independent solutions. This mesh was then subjected to time-step-interval independence test using time-step intervals of 0.02 s, 0.01 s, and 0.005 s, and the results are given in Fig. 9 (b). In the test, wave and current conditions and particle released position were so selected that the particle would escape underneath the plastic collector, a situation suitable for testing sensitivity on time-step interval. The results show that there were very little different in particle tracks until the particle hit the skirt of plastic collector. Downstream the skirt, the tracks returned by 0.01 s and 0.005 s were still very close to each other, while that of 0.02 s veered away. This

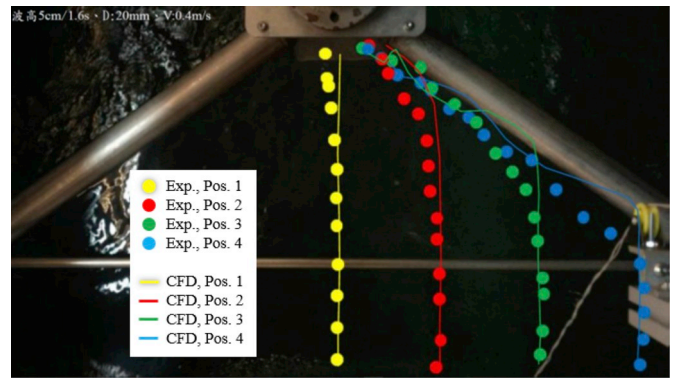
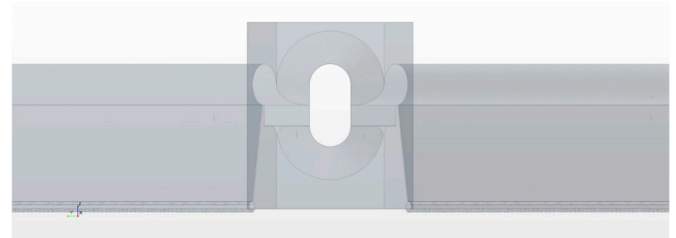


Fig. 10. Comparison of experimental and numerical particle tracks.



(a) Overall view of the full-scale collector.



(b) Enlarged view of the full-scale collector.

Fig. 11. The geometry of the full-scale collector; (a) overall view of the full-scale collector, (b) enlarged view of the full-scale collector.

indicates that the time-step interval of 0.01 s is good enough to achieve time-step-interval independence solutions. Therefore, the results obtained by the mesh of 5,700,000 cells with time-step interval of 0.01 s were used to compare with the experimental data.

Fig. 10 show the comparison of the tracks of particles released respectively from the four release positions between experiment and numerical simulation. The plot indicates that all particles, experimental and numerical, eventually entered the central collection hole, proving the accuracy in prediction of particle catch rate by the numerical simulation. It is also noticeable that the numerical tracks originated from release positions 1 and 2 are close to the experimental tracks. The deviation of the track path between experiment and numerical simulation is generally larger near the boom, where particles tracks were observed to be winding while particles were traveling along the boom towards the central hole. Both experimental and numerical tracks exhibit such behavior. This behavior is due to the stronger reflection waves near the boom that can temporarily push particles away from the boom. The reason for the deviation in the particle tracks by the experiment and the numerical simulation could be rooted in the unsteadiness of experimental waves whose variations in wave height can be as high as 8%. In contrast, all the characteristics of numerical waves were steady and perfectly equal. Since the present flow is a highly transient problem, a small deviation caused by the unsteadiness in waves at an upstream location can result in much larger differences in tracks at downstream locations. Overall, the numerical tracks agree reasonably well with the

Table 1
Operation conditions of the full-scale ocean plastic collector.

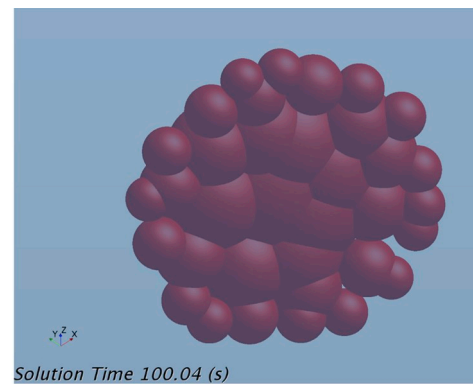
Case number	Current speed (ms^{-1})	Wave height (m)	Wave length (m)	Plastic density (kgm^{-3})	Catch rate (%)
1	0.5	0.4	5.0	900	100
2	1.0	0.4	5.0	900	100
3	1.5	0.4	5.0	900	100
4	1.5	0.1	5.0	900	100
5	1.5	0.3	5.0	900	100
6	1.5	0.5	5.0	900	100
7	1.5	0.4	2.0	900	100
8	1.5	0.4	4.0	900	100
9	1.5	0.4	6.0	900	100
10	1.5	0.4	8.0	900	100
11	1.5	0.4	10.0	900	100
12	1.5	0.4	5.0	800	100
13	1.5	0.4	5.0	980	100
14	2.0	1.2	2.0	900	100
15	2.0	1.2	4.0	900	100
16	2.0	0.2	5.0	900	100
17	2.0	0.4	5.0	900	100
18	2.0	0.6	5.0	900	91.0
19	2.0	0.8	5.0	900	100
20	2.0	1.0	5.0	900	100
21	2.0	1.2	5.0	900	8.24
22	2.5	0.4	5.0	900	100
23	2.5	0.6	5.0	900	91.26
24	2.5	0.8	5.0	900	32.03
25	2.5	1.0	5.0	900	88.34
26	2.5	1.2	5.0	900	7.5
27	3.0	0.4	5.0	900	100
28	3.0	0.6	5.0	900	45.63
29	3.0	0.8	5.0	900	50.48
30	3.0	1.0	5.0	900	42.71
31	3.0	1.2	5.0	900	1.94
32	3.5	0.4	5.0	900	89.32
33	3.5	0.6	5.0	900	24.27
34	3.5	0.8	5.0	900	65.04
35	3.5	1.0	5.0	900	28.15
36	3.5	1.2	5.0	900	0.97
37	4.0	0.4	5.0	900	4.85
38	4.0	0.6	5.0	900	10.67

experimental tracks, and the predicted particle catch rate is the same as the experiment; thus, the correctness of the current numerical approach, especially in predicting catch rate, has been validated.

4.2. Full-scale ocean plastic collector

Once the correctness of the numerical approach has been verified, attention was directed towards full scale simulation to assess the performance of the present collector design. Fig. 11 (a) illustrates the geometry of the full-scale ocean plastic collector model. Its geometry is similar to the scaled model but is 33 times larger in size. The boom has been extended and is 40 m in length. The length of the open front of the collector, that is from one boom's end to the other's end, is 70 m. The diameter of the boom is 1 m. The width of the skirt is 2.4 m, and it is tilted 10° backwards just like the scaled model. As shown in Fig. 11 (b), the central hole is shaped like a race track and is 1 m in width and 2 m in height. The ocean waves adopted in the simulation were "fifth-order" waves, which are closer to real ocean waves (Fenton, 1985).

There are many parameters that can affect the catch rate of an ocean plastic collector, for example, wind speed, ocean current speed, wave length, wave height, ocean depth, collector boom angle, or even the density of the plastic debris. Given the current problem is a transient problem with a typical solution time scale of 100 s and a time step of 0.01 s, to investigate the effects of so many different parameters would require very huge computer resources. Therefore, some simplification measures were implemented to reduce the number of parameters. First, wind speed and ocean current speed were assumed identical; hence there is only one variable for the two parameters. Second, the collector



(a) Plastic particle geometry



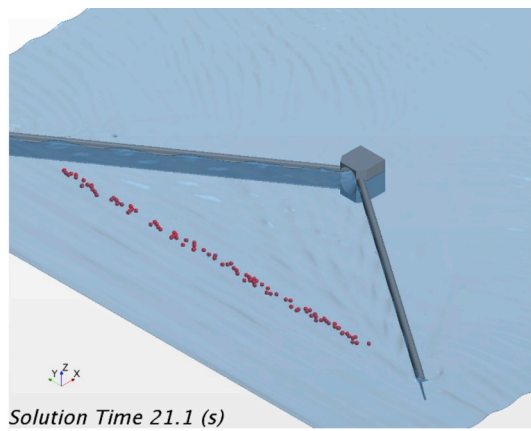
(b) Plastic particle release positions

Fig. 12. Plastic particles release positions; (a) plastic particle geometry, (b) plastic particle release positions.

was assumed to be deployed off shore in deep water, the water depth was kept constant. Third, the boom angle was fixed at 35° . In summary, only the effects of four parameters have been investigated here, namely, wind/ocean-current speed, wave height, wave length, and plastic density. Table 1 lists the conditions of all test cases of the full-scale model. There are 38 test cases, and the ranges of wind/ocean-current speed, wave height, wave length, and plastic density in these cases are 0.5 ms^{-1} to 4.0 ms^{-1} , 0.1 m–1.2 m, and 2 m–10 m, 800 kgm^{-3} to 980 kgm^{-3} , respectively. Among these cases, Cases 1–6 are in calm sea conditions with small current speed and wave height; Cases 7–11 are designated to investigate the effect of wave length; Cases 12–14 are for examining the effect of plastic density; and the rest of cases are for testing rougher sea conditions with larger current speed and wave height.

The mesh used for the full-scale study consists of 4,099,421 cells. This mesh has been determined after another grid-independence test on the full-scale model. Fig. 12 shows plastic particles' geometry and their release positions. As shown in Fig. 12 (a), a single plastic particle consists of 36 spheres in different diameters, collectively forming an irregular shape with a width of 0.1 m across. In Fig. 12 (b), there are 100 release positions, and they are evenly distributed along a line located 27 m in front of the central collection hole. Plastic particles were released 20 s after the start of simulation, allowing the flow field to be well developed and being free of initial-condition effect. In each test case, a total number of 100 plastic particles were released in a period of 1 s. A simulation would continue until all particles either passed the central hole or escaped over or underneath the collector unit.

Since plastic particle catch rate is the most important quantity to assess the collector's performance, the conditions listed in Table 1 can be classified into "high-catch-rate" and "low-catch-rate" conditions. In high-catch-rate conditions, the first 14 cases, ocean current speed is generally slow, and wave height is small. Fig. 13 illustrates plastic particles distributions at three moments in Case 3, which is a typical case in the high-catch-rate category. In these cases, the waves wouldn't flow over the top of the booms, and plastic particles were floating on water surface most of the time. Since plastic particles were moving slowly due to low current speed, they carried less momentum, and their flow path



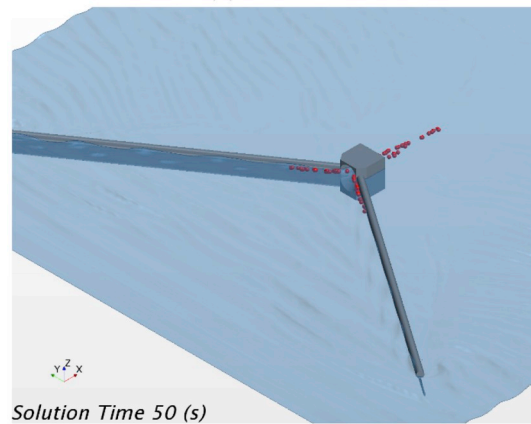
Solution Time 21.1 (s)

(a) $t=21.1$ s



Solution Time 39 (s)

(b) $t=39.0$ s

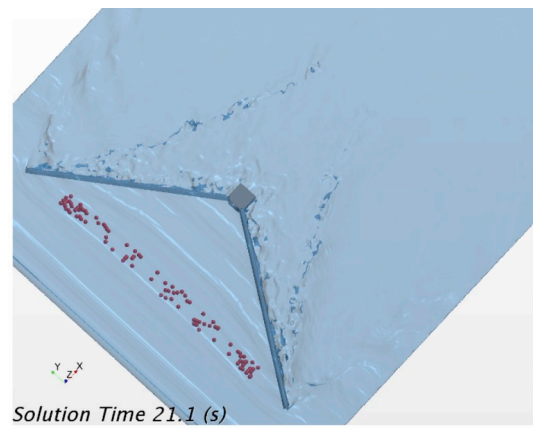


Solution Time 50 (s)

(c) $t=50.0$ s

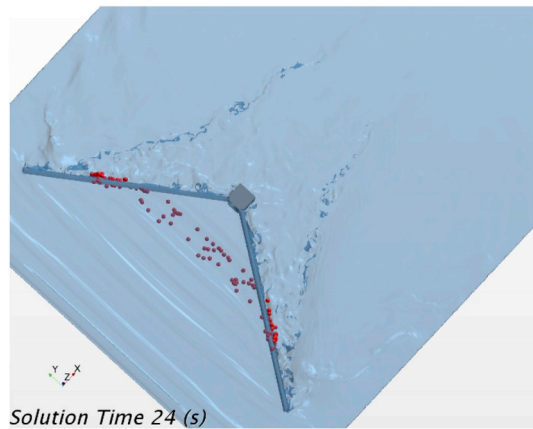
Fig. 13. Particle distributions at three moments in Case3; (a) $t=21.1$ s, (b) $t=39.0$ s, (c) $t=50.0$ s.

was strongly influenced by water surface flow. It is observable in Fig. 13 (b) that the booms of the collector forced the water surface flow to converge towards the central collection hole, and there went with the plastic particles which also converged towards the collection hole as they were drifted forwards. Eventually, they all passed the collection hole in an orderly way that those particles originated from the center of release line went in first, and those near the edges of the release line went in last (see Fig. 13 (c)). It is also worth noting that the catch rates of Cases 7–14 are all 100%, indicating that the parameters of wave length and plastic density only play minor roles on catch rate; hence the



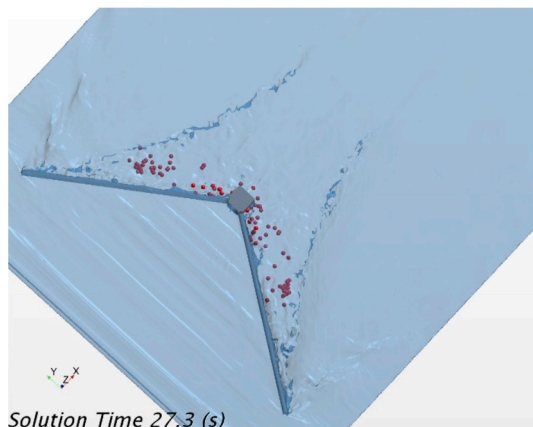
Solution Time 21.1 (s)

(a) $t=21.1$ s



Solution Time 24 (s)

(b) $t=24$ s



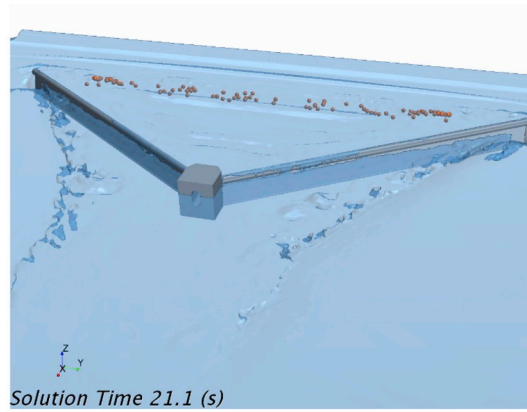
Solution Time 27.3 (s)

(c) $t=27.3$ s

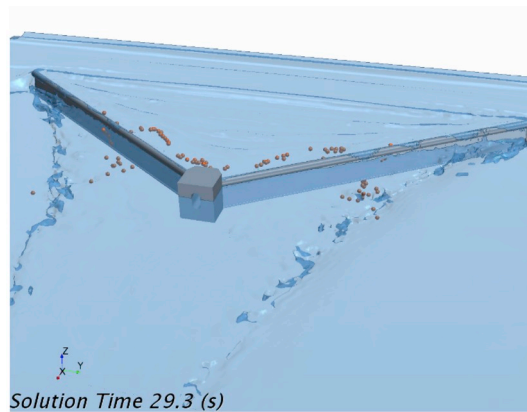
Fig. 14. Particle distributions at three moments in Case 38; (a) $t=21.1$ s, (b) $t=24.0$ s, (c) $t=27.3$ s.

following discussion will be focused on the influence imposed by ocean current speed and wave height.

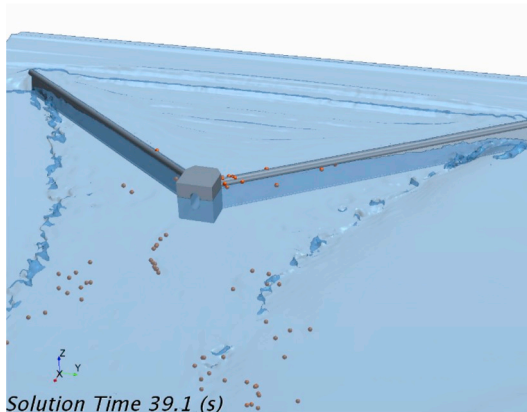
Figs. 14 and 15 respectively depict particle distributions in Case 38 and Case 36, both of which are in the low-catch-rate category. In this category, the ocean current speed is generally high, and wave height is also large. As the current speed increased, both water and plastic particles were moving at higher speed; hence they carried larger momentum which can easily overwhelm the barrier presented by the booms. Fig. 14 (b) and (c) indicate that surface water and most of the



(a) $t=21.1$ s



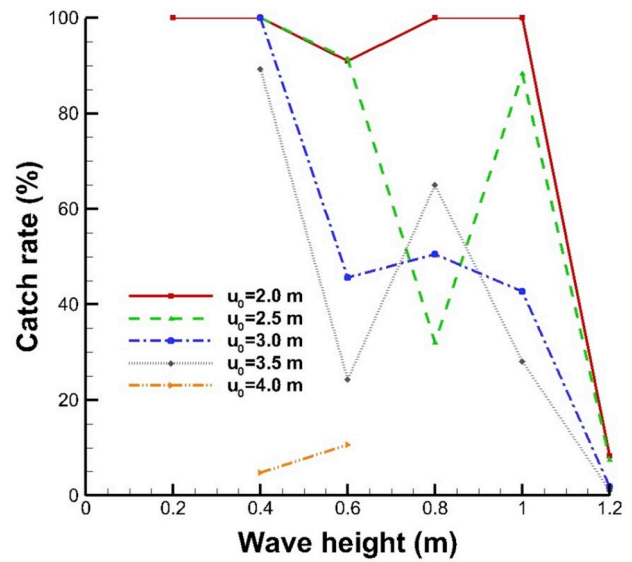
(b) $t=29.3$ s



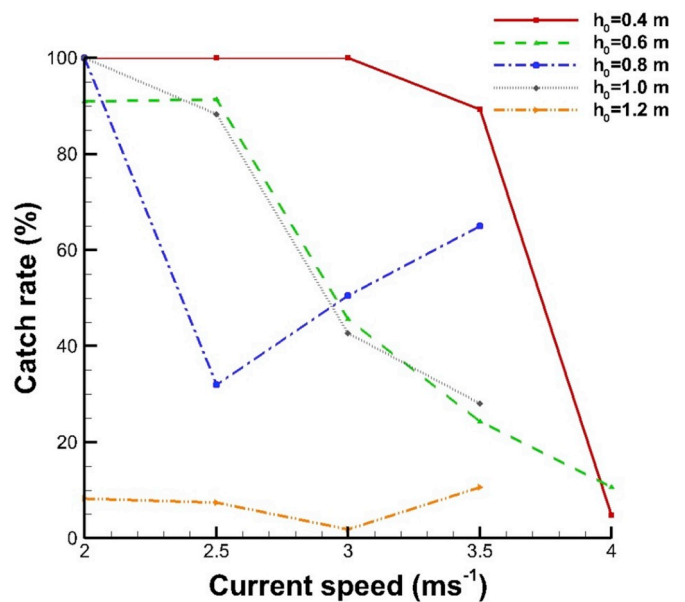
(c) $t=39.1$ s

Fig. 15. Particle distributions at three moments in Case 36; (a) $t = 21.1$ s, (b) $t = 29.3$ s, (c) $t = 39.1$ s.

plastic particles simply flew across the top of the booms. Furthermore, as demonstrated in Fig. 15 (b) and (c), strong current and large wave height could result in another scenario that particles flew underneath the skirts of the booms. In this scenario, the large wave height drove the particles to move up and down in larger magnitude. These particles thus possessed higher vertical momentum and could momentarily dive into water. Meanwhile, as the current flow reached the boom, it tended to split into two streams, one flowing over the top of the boom and the other flowing underneath the boom skirt. If the diving of a particle happened just before it approached a boom, the particle could be carried by the underneath stream and escaped the boom barrier by going underneath the boom skirt. The two cases demonstrate how unstable and



(a) Effects of wave height



(b) Effects of ocean current speed

Fig. 16. Effects of wave height and ocean current speed on catch rate; (a) effects of wave height, (b) effects of ocean current speed.

complicated the flow field near the collector was. Such transient and highly unstable flow plus higher particle momentum makes a particle's flow path very unstable and unpredictable, suggesting that the catch rate is also difficult to predict.

Fig. 16 (a) and (b) respectively show the effects of wave height and current speed on catch rate. A general tendency concluded from the plots is that catch rate tends to drop as wave height or current speed increases. However, the red lines in both plots suggest that under very low current speed or wave height conditions, catch rate can remain at high level until some thresholds. The lowest lines in the two plots show that these thresholds are wave height of 1.2 m and current speed of 4.0 ms^{-1} . It is also noticeable that the catch rate is a highly non-linear function of wave height and current speed. Especially, the green and black lines in Fig. 16 (a) and the blue line in Fig. 16 (b) fluctuate up and down as wave height or current speed increases. Nevertheless, some

operation conditions that yield high catch rate can be found. These conditions are: wave height is less than 0.4 m and current speed is lower than 2.5 ms^{-1} .

5. Conclusions

A passive ocean plastic debris collector has been designed, and its performance under rough sea conditions was investigated by using a CFD method. A scaled-model experiment was conducted to provide data for validating the correctness of the CFD method. Compared with the experimental results, the CFD method was proven to predict plastic particle tracks with reasonable accuracy and be able to return accurate prediction on catch rate. Then the CFD method was used to study the performance of the full-scale ocean plastic collector. A total of 38 cases were setup to investigate the effects of four parameters, namely ocean current speed, wave height, wave length, and plastic density on the collector's catch rate. It was found that wave length and plastic density only exert little influence on catch rate; hence the attention was focused on the parameters of ocean current speed and wave height. Some conclusions regarding their effects on catch rate can be drawn as follows:

1. Under low current speed and small wave height conditions, the catch rate is 100%.
2. Catch rate remains at high level until thresholds of wave height equal 0.4 m and current speed equal 2.5 ms^{-1} are reached.
3. When wave height is 1.2 m, or current speed is 4.0 ms^{-1} , the catch rate is less than 10%.

Given ocean current speed is normally much less than 2.5 ms^{-1} (Statnikov, 2002), the results indicate that the present collector can perform well under high-current-speed conditions. However, the results seem to suggest that it cannot cope with large wave height. In the present ocean plastic collector, the booms are rigid, and the entire device is assumed to be anchored firmly, so it doesn't heave up and down with the waves. In a real situation, the booms are flexible and will heave up and down with the wave; hence the relative wave height between the booms and ocean waves is much smaller than the absolute wave height adopted in the present study. In the future, the performance of the ocean plastic collector will be investigated by a CFD method that takes the movement of the booms into account.

Acknowledgement

This work was supported by the Ministry of Science and Technology,

Republic of China, under the grant number MOST 107-2218-E-006-042. The authors are very grateful for the financial support. Thanks also go to Green Conservation Program and Tse-Xin Organic Agriculture Foundation for providing valuable information and pictures for this work.

Appendix A. Supplementary data

Supplementary data to this article can be found online at <https://doi.org/10.1016/j.oceaneng.2019.106243>.

References

- Atan, R., Finnegan, W., Nash, S., Goggins, J., 2019. The effect of arrays of energy converters on the nearshore wave climate. *Ocean. Eng.* 172, 373–384.
- Cundall, P.A., Strack, O.D.L., 1979. A discrete numerical model for granular assemblies. *Geotechnique* 163, 47–65.
- Derraik, J.G., 2002. The pollution of the marine environment by plastic debris: a review. *Mar. Pollut. Bull.* 44, 842–852.
- Europe, Plastic, 2013. Plastics – the Fact 2013: an Analysis of European Latest Plastics Production, Demand, and Waste Data. https://www.plasticseurope.org/application/files/7815/1689/9295/2013plastics_the_facts_PubOct2013.pdf.
- Fenton, J.D., 1985. A fifth-order Stokes theory for steady waves. *J. Waterw. Port. Coast. Ocean Eng.* 111, 216–243.
- Gaur, S., Deo, M.C., 2008. Real-time wave forecasting using genetic programming. *Ocean. Eng.* 35, 1166–1172.
- Hamza, S.B., Habli, S., Said, N.M., Bournot, H., Le Palec, G., 2015. Simulation of pollutant dispersion of a free surface flow in coastal water. *Ocean. Eng.* 108, 81–97.
- Lavers, J.L., Bond, A.L., 2017. Exceptional and rapid accumulation of anthropogenic debris on one of the world's most remote and pristine islands. *Proc. Natl. Acad. Sci.* 114 (23), 6052–6055.
- Lebreton, L., Slat, B., Ferrari, F., Sainte-Rose, B., Aitken, J., Marthouse, R., 2018. Evidence that the great pacific garbage Patch is rapidly accumulating plastic. *Sci. Rep.* 8, 4666.
- Menter, F.R., 1994. Two-equation eddy-viscosity turbulence models for engineering applications. *AIAA J.* 32, 1598–1605.
- Menter, F.R., Kuntz, M., Langtry, R., 2003. Ten years of industrial experience with the SST turbulence model. *Turbul. Heat Mass Transf.* 4, 625–632.
- Moore, C.J., Phillips, C., 2011. Plastics ocean: How a sea captain's chance discovery launched a determined quest to save the oceans. *Avery Book*.
- Parker, L., 2014. The Best Way to Deal with Ocean Trash. <https://news.nationalgeographic.com/news/2014/04/140414-ocean-garbage-patch-plastic-pacific-debris>.
- Perkins, S., 2015. Nearly Every Seabird May Be Eating Plastic by 2050.
- Slat, B., 2014. How the Ocean Can Clean Themselves, a Feasibility Study. *The Ocean Cleanup Foundation*.
- Staedter, T., 2017. Humans Have Produced a Whopping 9 Billion Tons of Plastic. <https://www.livescience.com/59862-humans-have-produced-9-billion-tons-of-plastic.html>.
- Statnikov, E., 2002. Speed of ocean current. *The Physics Factbook*. <https://hypertextbook.com/facts/2002/EugeneStatnikov.shtml>.
- Wilcox, D.C., 1988. Reassessment of the scale-determining equation for advanced turbulence models. *AIAA J.* 26, 1299–1310.